NASA TR R-129

NATIONAL AERONAUTICS AND SPACE ADMINISTRATION

TECHNICAL REPORT
R-129

A THEORETICAL STUDY OF THE TORQUES INDUCED BY A MAGNETIC FIELD ON ROTATING CYLINDERS AND SPINNING THIN-WALL CONES, CONE FRUSTUMS, AND GENERAL BODY OF REVOLUTION

By G. LOUIS SMITH

1962

For sale by the Superintendent of Documents, U.S. Government Printing Office, Washington 25, D.C. Yearly subscription, $15: foreign, $19; single copy price varies according to size ---------- Price 30 cents

Code 1

SINGLE COPY ONLY

TECHNICAL REPORT R-129

A THEORETICAL STUDY OF THE TORQUES INDUCED BY A MAGNETIC FIELD ON ROTATING CYLINDERS AND SPINNING THIN-WALL CONES, CONE FRUSTUMS, AND GENERAL BODY OF REVOLUTION

By G. LOUIS SMITH

Langley Research Center
Langley Station, Hampton, Va.

TECHNICAL REPORT R–129

A THEORETICAL STUDY OF THE TORQUES INDUCED BY A MAGNETIC FIELD ON ROTATING CYLINDERS AND SPINNING THIN-WALL CONES, CONE FRUSTUMS, AND GENERAL BODY OF REVOLUTION

By G. Louis Smith

SUMMARY

The electromagnetic field equations are applied to nonferromagnetic conducting slowly spinning thin- and thick-wall open-ended cylinders and thin-wall cone frustums, and also to thin-wall tumbling cylinders, to calculate the induced eddy currents from which the resulting torques are determined. A method is also presented for determining the eddy currents, and hence the torque, in a series of cone frustums joined end to end. When applied to the limiting case, this method leads to the solution for the general body of revolution.

Figures that show the variation of torque with fineness ratio and thickness ratio are presented for thin- and thick-wall cylinders. The torque acting on a tumbling cylinder was found to be one-half the torque acting on a symmetrically spinning cylinder, all other factors being equal. Results from this analysis are directly applicable to calculations of the torque acting on spinning and tumbling satellites.

INTRODUCTION

One of the many considerations in dealing with satellites is the interaction of the earth's magnetic field with the conducting shell of a spinning satellite. (See refs. 1 to 4.) The geomagnetic field induces eddy currents within the rotating conducting shell, which in turn interact with the field to produce a torque. One component of this torque slows the rotation, and another component tends to precess the direction of the spin axis. (See ref. 4.)

In studying this interaction analytically, it is necessary to apply Maxwell's electromagnetic field equations with the appropriate boundary conditions to the problem. The solution for a sphere, which is applicable to spherical shells such as those of the Vanguard series of satellites, has been presented in references 4 and 5. The purpose of this paper is to present the solutions for some other configurations. Two cylinder cases are solved: the cylinder spinning about its center line and the cylinder spinning about an axis perpendicular to the center line. All rotations can be resolved into these two components. The importance of having both solutions available for the general cylindrical satellite is that, although it may be injected into orbit spinning about the axis of minimum moment of inertia, internal dissipation of kinetic energy causes the spin axis eventually to shift to the axis of maximum moment of inertia.

Thin cones and frustums of cones are also investigated and equations are derived for the induced currents within the shell, from which the torque follows. A method is set up for extending these results to a series of frustums joined together. This method leads to a solution for a general body of revolution.

In each case, equations are derived for the current density throughout the body and for the total resultant torque.

SYMBOLS

C	curve of integration
c	velocity of light
$\mathbf{E}$	electric field intensity vector

E (with subscript) component of $\mathbf{E}$
$\mathbf{e}_1, \mathbf{e}_2, \mathbf{e}_3$ unit vectors along ξ, η, and ζ axes
$\mathbf{F}$ vector force per unit volume
$\mathbf{H}$ magnetic field intensity vector
h magnitude of $\mathbf{H}$
$\mathbf{i}, \mathbf{j}, \mathbf{k}$ unit vectors along X, Y, and Z axes
$\mathbf{J}$ current density vector
J (with subscript) component of $\mathbf{J}$
$J_n(\ )$ Bessel function of first kind, of order n
k_m, k_{mn} eigenvalues in thick-wall cylinder solution
$\mathbf{L}$ torque vector
l length of cylinder
$P(x)$ function defined by equation (36)
$\mathbf{r}$ radius vector
r radius (cylindrical coordinate)
t time
$\mathbf{u}$ (with subscript) unit vector, in direction indicated
w transformation variable, defined by equation (71)
x, y, z distance along coordinate axes X, Y, and Z
$Y_n(\ )$ Bessel function of second kind, of order n
$Z_n(\ )$ cylinder function of order n, $E_{mn}J_n(\ )+F_{mn}Y_n(\ )$
α_m quantities defined by equation (40)
β_m quantities defined by equation (46)
θ angle from X-axis in X,Y plane (cylindrical and spherical coordinate)
λ angle between Z-axis and $\mathbf{H}$
μ angle defined in figure 10 for tumbling-cylinder analysis
ν polar angle in plane, used in cone analysis
ξ, η, ζ coordinate axes used in analysis of tumbling cylinder (see fig. 10)
ρ distance along cone from vertex to point (spherical coordinate)
σ electrical conductivity
τ thickness of thin wall
Φ harmonic function; for example, equation (13)
ϕ cone half-angle (fig. 11)
ψ stream function
$\boldsymbol{\omega}$ spin vector
ω spin rate

Subscripts:

a, b quantity evaluated at end a or end b
i inside
o outside
av average

GOVERNING EQUATIONS AND BOUNDARY CONDITIONS

In order to formulate the problem mathematically, it is necessary first to list the equations and the boundary conditions to be used. Maxwell's equations describe the magnetic and electric fields inside and outside the cylinder. (See refs. 4 and 6.) The analysis is restricted to nonferromagnetic metals so that, in Gaussian units, the permittivity and permeability are near unity. Also, for spin rates reasonable for most satellites, the magnetic field due to the induced eddy currents is small compared with the primary field; therefore, the unperturbed magnetic field can be used in the electric field equations. This approximation is justified in reference 4. Also, for spin rates of the magnitude applicable to satellites, the charge density within a conductor will be negligible. Thus, as is shown in reference 4, the electric field equations are

$$\nabla\times\mathbf{E}=-c^{-1}\frac{\partial\mathbf{H}}{\partial t} \tag{1}$$

$$\nabla\cdot\mathbf{E}=0 \tag{2}$$

In stationary axes, the electric field can be written (ref. 4) as:

$$\mathbf{E}=\nabla\Phi+c^{-1}(\boldsymbol{\omega}\times\mathbf{r})\times\mathbf{H} \tag{3}$$

where $\nabla^2\Phi=0$, and Φ, the potential of the electric field, is determined by the boundary conditions. The term $c^{-1}(\boldsymbol{\omega}\times\mathbf{r})\times\mathbf{H}$ is the induced electric field. The current follows immediately from

$$\mathbf{J}=\sigma\mathbf{E} \tag{4}$$

The force per unit volume is then

$$\mathbf{F}=c^{-1}\mathbf{J}\times\mathbf{H} \tag{5}$$

and the torque is calculated by integrating the differential torque

$$d\mathbf{L}=\mathbf{r}\times d\mathbf{F} \tag{6}$$

The only boundary condition is that the component of current (or electric field) normal to the surface vanish at the surface. This condition, together with the induced field, is sufficient to determine Φ and $\nabla\Phi$ completely.

Equation (3) is well suited for calculating the electric field in symmetrically spinning cylinders,

inasmuch as the boundary condition can be readily applied in this case to determine Φ; it will be used in the study of both symmetrically spinning thin-wall and thick-wall cylinders. However, in calculating the electric field in thin-wall tumbling cylinders and spinning cones, equation (3) is not so well suited, and it becomes convenient to use a stream function to solve equations (1) and (2) simultaneously.

SYMMETRICALLY SPINNING CYLINDER

For the symmetrically spinning cylinder, an approximate solution is first obtained for the thin-wall shells. The solution for the thick-wall cylinder is then derived, and a comparison is made of the two solutions.

To study the case of a symmetrically spinning open-ended cylinder, Cartesian and cylindrical coordinate systems are first set up as shown in figure 1. The Z-axis is set up along the center line of the cylinder, and the X-axis is defined in such a way that $\mathbf{H}$ lies in the X, Z plane and forms an angle λ with the Z-axis. The quantities $\mathbf{H}$, $\mathbf{r}$, and $\boldsymbol{\omega}$ can then be written as

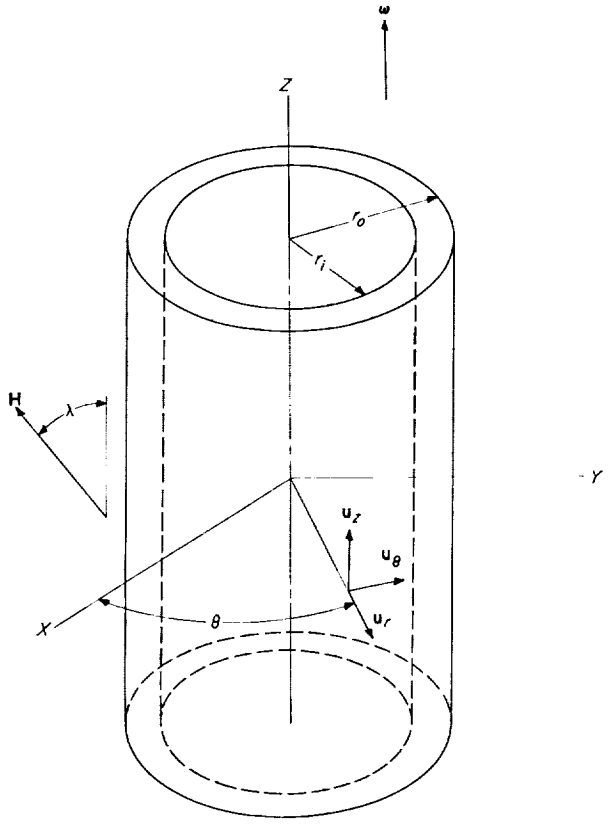

FIGURE 1.—Coordinate systems for symmetrically spinning cylinder.

$$\mathbf{H}=h(\mathbf{i}\sin\lambda+\mathbf{k}\cos\lambda)$$

$$=h(\mathbf{u}_r\sin\lambda\cos\theta-\mathbf{u}_\theta\sin\lambda\sin\theta+\mathbf{u}_z\cos\lambda) \quad (7)$$

$$\mathbf{r}=\mathbf{u}_r r+\mathbf{u}_z z \quad (8)$$

$$\boldsymbol{\omega}=\mathbf{u}_z\omega \quad (9)$$

Equation (3) thus becomes

$$\mathbf{E}=\nabla\Phi+c^{-1}h\omega r(\mathbf{u}_r\cos\lambda-\mathbf{u}_z\sin\lambda\cos\theta) \quad (10)$$

The boundary conditions may then be written as

$$E_z\left(r,\theta,\pm\frac{l}{2}\right)=0 \quad (11)$$

$$E_r(r_i,\theta,z)=E_r(r_o,\theta,z)=0 \quad (12)$$

THIN-WALL CASE

For a thin-wall open-ended cylindrical shell, the radial component of flow will be negligible by comparison with the circumferential and longitudinal components, J_θ and J_z, respectively, and J_θ and J_z will not vary significantly between $r=r_i$ and $r=r_o$. The problem therefore can be considered to be primarily dependent on θ and z. Since the cylinder can then be cut along an element and developed onto a plane, the problem may be treated as two-dimensional, with $r\theta$ as the abscissa and z as the ordinate, where r is taken to be the "average" radius. Only a strip of the plane one period in width need be considered. A potential field $\nabla\Phi$ is now superimposed on the field and adjusted to make the longitudinal components of the total field vanish at the boundaries of the region corresponding to the open ends of the cylinder. The potential then is

$$\Phi=\sum_{n=0}^{\infty}(A_n\sin n\theta+B_n\cos n\theta)\left(C_n\sinh\frac{nz}{r}+D_n\cosh\frac{nz}{r}\right) \quad (13)$$

Equation (10) thus becomes

$$\mathbf{E}=-\mathbf{u}_z c^{-1}h\omega r\sin\lambda\cos\theta+\mathbf{u}_z\sum_{n=0}^{\infty}(A_n\sin n\theta+B_n\cos n\theta)\left(C_n\cosh\frac{nz}{r}+D_n\sinh\frac{nz}{r}\right)\frac{n}{r}+\frac{\mathbf{u}_\theta}{r}\sum_{n=0}^{\infty}n(A_n\cos n\theta-B_n\sin n\theta)\left(C_n\sinh\frac{nz}{r}+D_n\cosh\frac{nz}{r}\right) \quad (14)$$

The radial components have been dropped in equation (14) for this thin-wall case; thus, equations (12) are satisfied automatically. In order to satisfy the boundary condition (11), it is necessary that the first term of equation (14) cancel the first summation at $z=\pm\frac{l}{2}$. This is easily accomplished by letting all the coefficients be zero except B_1 and C_1. Then

$$0=-c^{-1}h\omega r\sin\lambda\cos\theta+\frac{B_1C_1}{r}\cos\theta\cosh\frac{l}{2r}$$

from which

$$B_1C_1=\frac{c^{-1}h\omega r^2\sin\lambda}{\cosh\frac{l}{2r}} \tag{15}$$

Substituting equation (15) into equation (13) gives the potential as

$$\Phi(\theta,z)=c^{-1}h\omega r^2\sin\lambda\cos\theta\frac{\sinh\frac{z}{r}}{\cosh\frac{l}{2r}} \tag{16}$$

The electric field is then

$$\mathbf{E}(\theta,z)=-\mathbf{u}_z c^{-1}h\omega r\sin\lambda\cos\theta\left(1-\frac{\cosh\frac{z}{r}}{\cosh\frac{l}{2r}}\right)$$

$$-\mathbf{u}_\theta c^{-1}h\omega r\sin\lambda\sin\theta\frac{\sinh\frac{z}{r}}{\cosh\frac{l}{2r}} \tag{17}$$

The electric field having been determined, the current follows immediately by equation (4). The torque is then calculated by

$$\mathbf{L}=c^{-1}\int_V\mathbf{r}\times(\mathbf{J}\times\mathbf{H})dV \tag{18}$$

where V is volume. Equations (7), (8), and (17) are substituted into the integrand of equation (18). The resulting vector expression in terms of $\mathbf{u}_r$, $\mathbf{u}_\theta$, and $\mathbf{u}_z$ is then referred to the X,Y,Z system in terms of $\mathbf{i}$, $\mathbf{j}$, and $\mathbf{k}$. The result is then integrated over the surface of the cylinder. (Because of the thin-wall approximations, the integration with respect to r is replaced by simply multiplying by the thickness τ.) The final result is

$$\mathbf{L}=\pi\sigma c^{-2}h^2\omega\sin\lambda r^3l\tau\left(1-\frac{2r}{l}\tanh\frac{l}{2r}\right)$$

$$(\mathbf{i}\cos\lambda-\mathbf{k}\sin\lambda) \tag{19}$$

The factor $1-\frac{2r}{l}\tanh\frac{l}{2r}$, which is the torque per unit length normalized with respect to the torque per unit length of a similar cylindrical shell of infinite length, is plotted as a function of fineness ratio in figure 2. It is seen from this figure that the torque per unit length varies rapidly with fineness ratio up to a ratio of approximately 5, after which the torque per unit length is a weak function of fineness ratio. The torque, similarly normalized, is shown in figure 3.

The conventional stream function ψ, describing the current paths within the cylindrical shell, is defined by

$$\left.\begin{aligned}\frac{\partial\psi}{r\partial\theta}&=J_z=\sigma E_z\\ \frac{\partial\psi}{\partial z}&=-J_\theta=-\sigma E_\theta\end{aligned}\right\} \tag{20}$$

Dimensionally, this definition corresponds to a

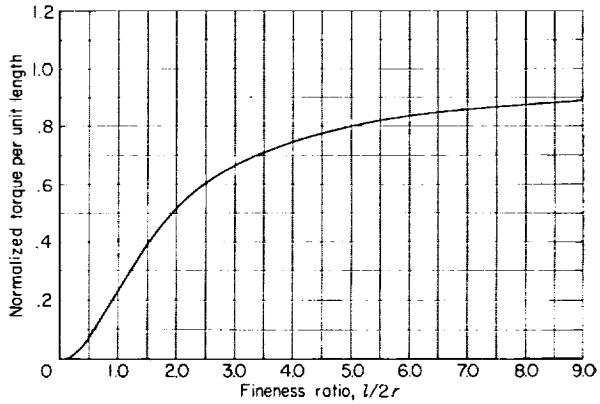

FIGURE 2.—Normalized torque per unit length as a function of fineness ratio for spinning thin-wall cylinder.

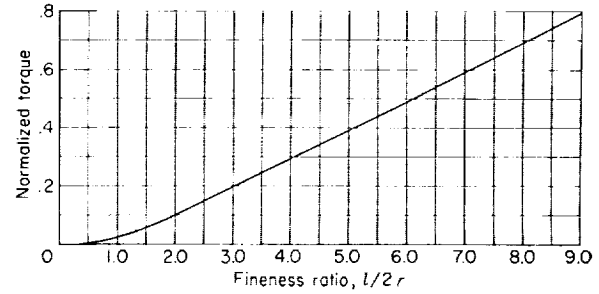

FIGURE 3.—Normalized torque as a function of fineness ratio for spinning thin-wall cylinder.

unit thickness. Then by equation (17)

$$\psi(\theta, z) = -\sigma c^{-1} h \omega r^2 \sin \lambda \sin \theta \left[1 - \frac{\cosh \frac{z}{r}}{\cosh \frac{l}{2r}} \right] \quad (21)$$

The current paths, or streamlines, are given by lines of constant ψ and are shown in figures 4(a), 4(b), and 4(c) for fineness ratios of 2, 4, and 8, respectively. The mapping for $\pi \leqq \theta \leqq 2\pi$ will be identical to that shown for $0 \leqq \theta \leqq \pi$. The values of ψ have been normalized by dividing by the maximum value. The direction of the flow depends, of course, on the relative direction of the spin vector and the applied magnetic field vector and thus is not indicated. Comparison of these figures shows physically why the torque per unit length varies as it does with fineness ratio. As the fineness ratio is increased, the current paths become more nearly straight and parallel, except near the ends; thus, in the limiting case of an infinite cylinder, the streamlines are parallel.

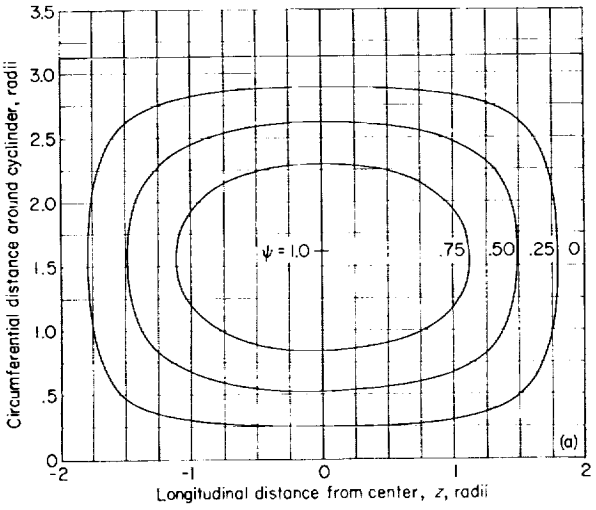

(a) Fineness ratio $\frac{l}{2r} = 2$.

FIGURE 4.—Current paths for spinning thin-wall cylinder.

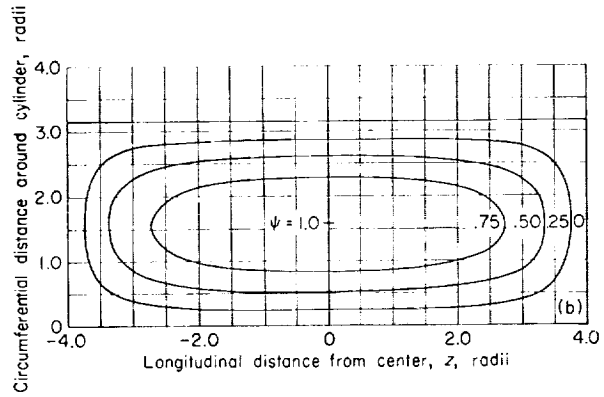

(b) Fineness ratio $\frac{l}{2r} = 4$.

FIGURE 4.—Continued.

In the preceding analysis the problem of the torque and eddy currents produced by a conducting cylindrical shell spinning in a magnetic field has been studied on the basis of thin-wall approximations. Exact solutions to the problem for a thick-wall cylinder will now be derived because of their intrinsic interest and also to substantiate the thin-wall treatment and to find its limitations.

THICK-WALL CASE

In order to determine the electric field within a thick-wall cylinder, equations (10) to (12) are again employed. The cylindrical harmonic may be written as

$$\Phi(r, \theta, z) = \sum_m \sum_n (A_{mn} \sinh k_{mn} z + B_{mn} \cosh k_{mn} z)(C_{mn} \sin n\theta + D_{mn} \cos n\theta) Z_n(k_{mn} r) + \sum_n (A_n \sin n\theta + B_n \cos n\theta)(C_n z + D_n)(E_n r^n + F_n r^{-n}) + C_0 \log_e r \quad (22)$$

where

$$Z_n(k_{mn} r) = E_{mn} J_n(k_{mn} r) + F_{mn} Y_n(k_{mn} r) \quad (23)$$

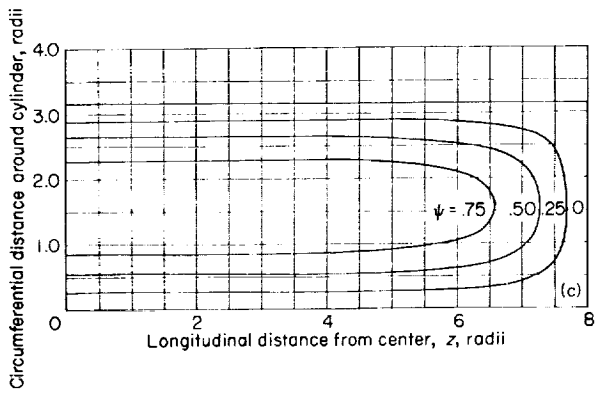

(c) Fineness ratio $\frac{l}{2r} = 8$.

FIGURE 4.—Concluded.

and $J_n(\ )$ and $Y_n(\ )$ are Bessel functions of order n of the first and second kinds, respectively. For simplicity, λ will be taken to be $\pi/2$. From physical considerations it is apparent that only the component of the magnetic field normal to the spin axis is effective in generating a current; therefore, this restriction on λ will be inconsequential. By using equations (10) and (22), the components of the electric field vector within the conductor can be written as

$$E_r=\frac{\partial\Phi}{\partial r}$$
$$=\sum_m\sum_n (A_{mn}\sinh k_{mn}z + B_{mn}\cosh k_{mn}z)(C_{mn}\sin n\theta + D_{mn}\cos n\theta)Z_n'(k_{mn}r)+\sum_n(A_n\sin n\theta + B_n\cos n\theta)(C_nz+D_n)(E_nr^{n-1} - F_nr^{-n-1})n+\frac{C_o}{r} \quad (24)$$

$$E_\theta=\frac{\partial\Phi}{r\partial\theta}$$
$$=\frac{1}{r}\sum_m\sum_n (A_{mn}\sinh k_{mn}z + B_{mn}\cosh k_{mn}z)(C_{mn}\cos n\theta - D_{mn}\sin n\theta)nZ_n(k_{mn}r) + \frac{1}{r}\sum_n (A_n\cos n\theta - B_n\sin n\theta)(C_nz + D_n)(E_nr^n + Fr^{-n})n \quad (25)$$

$$E_z=\frac{\partial\Phi}{\partial z}-c^{-1}h\omega r\cos\theta$$
$$=\sum_m\sum_n k_{mn}(A_{mn}\cosh k_{mn}z + B_{mn}\sinh k_{mn}z)(C_{mn}\sin n\theta + D_{mn}\cos n\theta)Z_n(k_{mn}r) + \sum_n C_n(A_n\sin n\theta + B_n\cos n\theta)(E_nr^n + F_nr^{-n}) - c^{-1}h\omega r\cos\theta \quad (26)$$

The boundary conditions are now applied to the problem. First the requirement of equation (11) that the longitudinal component of the electric field vanish at the ends is applied to equation (26). By symmetry $B_{mn}=0$. Also, only the $\cos\theta$ terms can have nontrivial coefficients, that is, $D_{mn}=B_n=0$ $(n\neq 1)$ and $C_{mn}=A_n=0$. Next, the requirement of equation (12) that the radial component of the electric field vanish at the inside and outside surfaces is applied to equation (24). This condition gives $C_o=0$, $E_n=F_n=0$, and

$$Z_n'(k_{mn}r_o)=Z_n'(k_{mn}r_i)=0 \quad (27)$$

Equations (27) yield the characteristic equation which determines the eigenvalues k_{mn} and also $\frac{F_{mn}}{E_{mn}}$. The method of evaluating them will be discussed presently. By letting $D_{m1}=1$ and dropping the n subscript, equations (22), (24), (25), and (26) are reduced to

$$\Phi(r,\theta,z)=\sum_{m=1}^{\infty}A_m\sinh k_mz\cos\theta Z_1(k_mr) \quad (28)$$

$$E_r=\sum_{m=1}^{\infty}A_m\sinh k_mz\cos\theta Z_1'(k_mr) \quad (29)$$

$$E_\theta=-\sum_{m=1}^{\infty}A_m\sinh k_mz\sin\theta Z_1(k_mr) \quad (30)$$

$$E_z=\sum_{m=1}^{\infty}A_mk_m\cosh k_mz\cos\theta Z_1(k_mr)-c^{-1}h\omega r\cos\theta \quad (31)$$

In order to evaluate k_m and $\frac{F_{mn}}{E_{mn}}$, equation (27) is expanded by means of equation (23) and then $Z_1'(k_mr)$ is replaced by $k_mZ_o(k_mr)-\frac{1}{r}Z_1(k_mr)$. The following two equations are thus obtained:

$$E_m\left[k_mJ_o(k_mr_i)-\frac{1}{r_i}J_1(k_mr_i)\right] + F_m\left[k_mY_o(k_mr_i)-\frac{1}{r_i}Y_1(k_mr_i)\right]=0 \quad (32)$$

$$E_m\left[k_mJ_o(k_mr_o)-\frac{1}{r_o}J_1(k_mr_o)\right] + F_m\left[k_mY_o(k_mr_o)-\frac{1}{r_o}Y_1(k_mr_o)\right]=0 \quad (33)$$

Eliminating $\frac{F_m}{E_m}$ between equations (32) and (33) gives the characteristic equation for the k_m values:

$$\frac{k_mJ_o(k_mr_o)-\frac{1}{r_o}J_1(k_mr_o)}{k_mY_o(k_mr_o)-\frac{1}{r_o}Y_1(k_mr_o)}=\frac{k_mJ_o(k_mr_i)-\frac{1}{r_i}J_1(k_mr_i)}{k_mY_o(k_mr_i)-\frac{1}{r_i}Y_1(k_mr_i)} \quad (34)$$

One method of solving equation (34) is to rewrite it as

$$\frac{k_m r_o J_o(k_m r_o) - J_1(k_m r_o)}{k_m r_o Y_o(k_m r_o) - Y_1(k_m r_o)} = \frac{k_m r_i J_o(k_m r_i) - J_1(k_m r_i)}{k_m r_i Y_o(k_m r_i) - Y_1(k_m r_i)} \tag{35}$$

Now define $P(x)$ by

$$P(x) = \frac{x J_o(x) - J_1(x)}{x Y_o(x) - Y_1(x)} \tag{36}$$

Thus, the characteristic equation may be written as

$$P(k_m r_i) = P(k_m r_o) \tag{37}$$

A plot of the variation of $P(x)$ with x which is applicable for all cases can be made. To determine the eigenvalues for a cylinder with a given r_i/r_o, $P\left(\frac{r_i}{r_o}x\right)$ is plotted as a function of x. The intersections of $P\left(\frac{r_i}{r_o}x\right)$ with $P(x)$ satisfy equation (37) and therefore give the desired eigenvalues $k_m = \frac{x}{r_o}$. Such a plot is shown in figure 5. The solid line is for $P(x)$ and the dashed line is for $P(0.5x)$ or $\frac{r_i}{r_o} = 0.5$. In this example, the first three eigenvalues given by the intersections are seen to be $k_m = 1.42$, 6.53, and 12.65, where r_o is assumed to be unity. The variations of the first few eigenvalues with r_i/r_o are shown in figure 6.

After the eigenvalues have been determined, F_m/E_m is given immediately by

$$\frac{F_m}{E_m} = -P(k_m r_o) \tag{38}$$

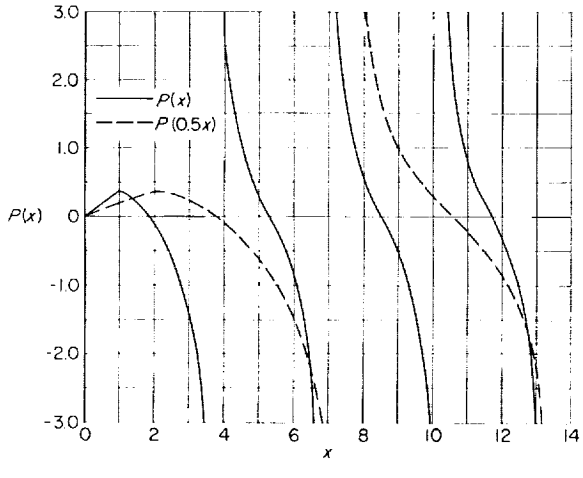

FIGURE 5.—Plot for graphical determination of eigenvalues.

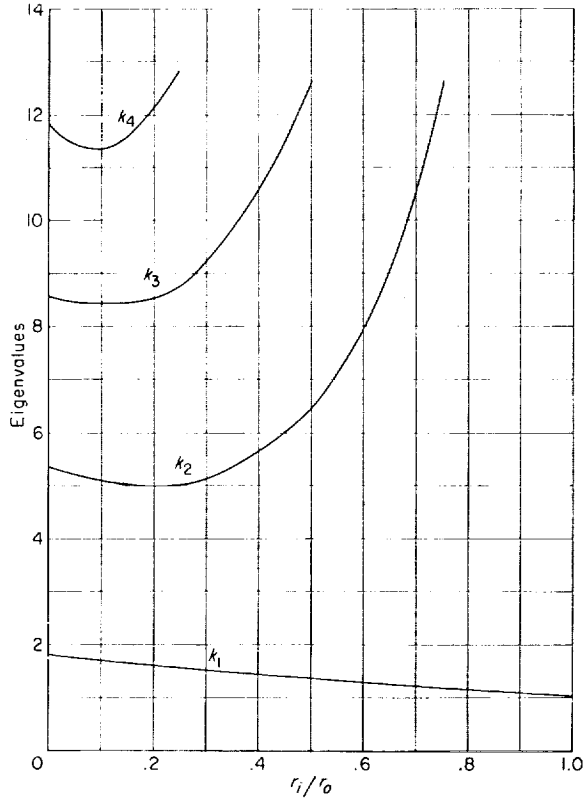

FIGURE 6.—Variation of eigenvalues with r_i/r_o.

The variation of the first few values of F_m/E_m with r_i/r_o is shown in figure 7. The singular points occur where E_m becomes zero while F_m remains finite.

The A_m values are determined by again applying equation (11) to equation (31) and using the orthogonality properties of Bessel functions:

$$A_m = \frac{c^{-1} h \omega r_o \alpha_m}{k_m \cosh \frac{k_m l}{2}} \tag{39}$$

where, by reference 7,

$$\alpha_m = \frac{\int_{r_i}^{r_o} r^2 Z_1(k_m r) dr}{r_o \int_{r_i}^{r_o} r [Z_1(k_m r)]^2 dr} = \frac{\frac{r^2}{k_m} Z_2(k_m r)\Big|_{r_i}^{r_o}}{r_o \frac{r^2}{2} \{[Z_1(k_m r)]^2 - Z_0(k_m r) Z_2(k_m r)\}\Big|_{r_i}^{r_o}} \tag{40}$$

The α_m values are thus nondimensional and are

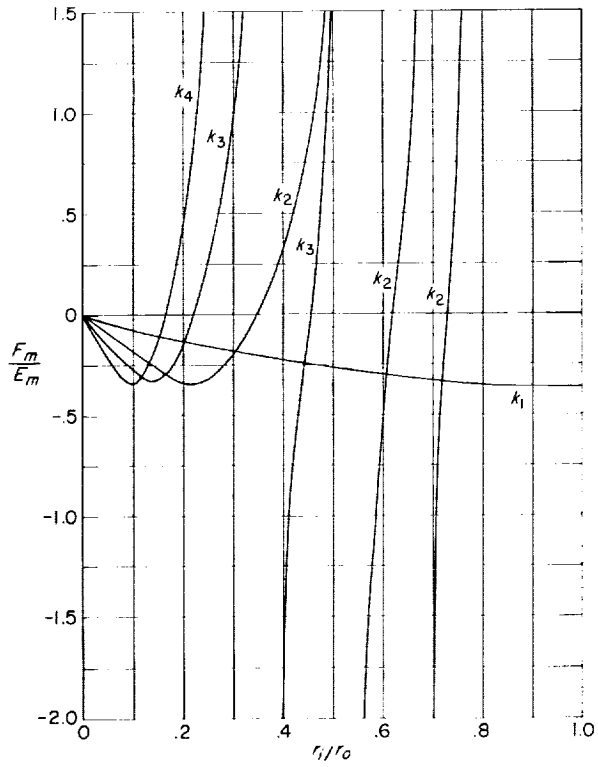

FIGURE 7.—Variation of F_m/E_m with r_i/r_o for different eigenvalues.

functions only of r_i/r_o for a given m. It is noted that E_m and F_m need not be separately determined; only their ratio F_m/E_m need be found. Substituting equation (39) into equations (28) to (31) gives

$$\Phi(r,\theta,z)=c^{-1}h\omega r_o\cos\theta\sum_{m=1}^{\infty}\frac{\alpha_m}{k_m}\frac{\sinh k_m z}{\cosh\frac{k_m l}{2}}Z_1(k_m r) \quad (41)$$

$$E_r=c^{-1}h\omega r_o\cos\theta\sum_{m=1}^{\infty}\frac{\alpha_m}{k_m}\frac{\sinh k_m z}{\cosh\frac{k_m l}{2}}Z_1'(k_m r) \quad (42)$$

$$E_\theta=-c^{-1}h\omega\frac{r_o}{r}\sin\theta\sum_{m=1}^{\infty}\frac{\alpha_m}{k_m}\frac{\sinh k_m z}{\cosh\frac{k_m l}{2}}Z_1(k_m r) \quad (43)$$

$$E_z=-c^{-1}h\omega r_o\cos\theta\left[\frac{r}{r_o}-\sum_{m=1}^{\infty}\alpha_m\frac{\cosh k_m z}{\cosh\frac{k_m l}{2}}Z_1(k_m r)\right] \quad (44)$$

The electric field is therefore determined within the cylinder. The convergence of these summations is generally good.

The procedure for determining the torque is essentially the same as outlined before for the thin-wall cylindrical shell. The result is

$$\mathbf{L}=\pi\sigma c^{-2}h^2\sin\lambda\omega l r_o^4\left\{\frac{1}{4}\left[1-\left(\frac{r_i}{r_o}\right)^4\right]-\sum_{m=1}^{\infty}\frac{\beta_m}{k_m'\frac{l}{2r_o}}\tanh\left(k_m'\frac{l}{2r_o}\right)\right\}(\mathbf{i}\cos\lambda-\mathbf{k}\sin\lambda) \quad (45)$$

where $l/2r_o$ is the fineness ratio, k_m' is the eigenvalue nondimensionalized with respect to r_o, that is, $k_m'=r_o k_m$, and β_m is defined by

$$\beta_m=\frac{\alpha_m}{r_o^3}\int_{r_i}^{r_o}r^2 Z_1(k_m r)\,dr=\frac{\alpha_m}{r_o^3}\left[\frac{r^2}{k_m}Z_2(k_m r)\right]\Bigg|_{r_i}^{r_o} \quad (46)$$

Note that again, for large values of the fineness ratio $l/2r_o$, the torque per unit length is independent of the fineness ratio.

The torque per unit length per unit thickness as a function of r_i/r_o is shown in figure 8 for various fineness ratios. (The product $\sigma c^{-2}h^2\omega r_o^4$ is taken to be unity.) Figure 9 is a cross plot showing the torque per unit length per unit thickness as a function of fineness ratio for various r_i/r_o values. The $\frac{r_i}{r_o}=1.0$ curve is identical to that for the thin-wall solution shown in figure 2.

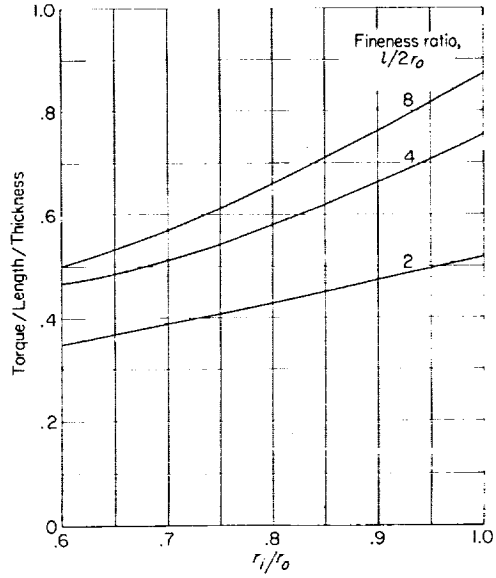

FIGURE 8.—Torque per unit length per unit thickness as a function of r_i/r_o for spinning thick-wall cylinder. The product $\sigma c^{-2}h^2\omega r_o^4$ is taken to be unity.

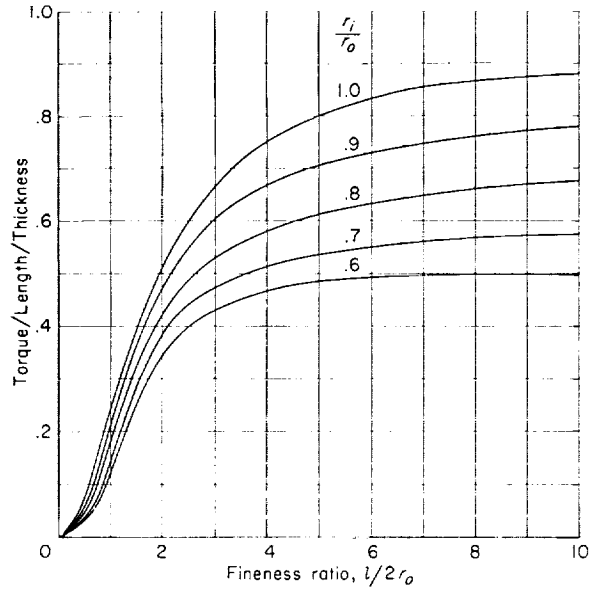

FIGURE 9.—Torque per unit length per unit thickness as a function of fineness ratio for spinning thick-wall cylinder. The product $\sigma c^{-2}h^2\omega r_o^4$ is taken to be unity.

THIN-WALL TUMBLING CYLINDER

The coordinate systems used in the analysis of the tumbling cylinder are shown in figure 10. The ξ, η, ζ coordinate system, with the unit vectors $\mathbf{e}_1$, $\mathbf{e}_2$, and $\mathbf{e}_3$, is space fixed at the center of the rotating cylinder, with the ξ-axis parallel to the spin axis and the ζ-axis oriented so that the magnetic field vector lies in the ξ, ζ plane. The X, Y, Z system with unit vectors $\mathbf{i}$, $\mathbf{j}$, and $\mathbf{k}$ is fixed in the cylinder with the origin at the center of the cylinder, the X-axis being alined with the ξ-axis, and is rotated from the space-fixed system by the angle μ. In addition, a polar coordinate system r, θ, z with unit vectors $\mathbf{u}_r$, $\mathbf{u}_\theta$, and $\mathbf{u}_z$ is fixed in the cylinder, θ being measured from the X-axis, as in figure 1.

Now, because only the normal component of $\nabla\times\mathbf{J}$ is effective in a thin-wall conductor and radial currents are negligible, equations (1) and (4) give for this case

$$(\nabla\times\mathbf{J})_r=\frac{\partial J_z}{r\partial\theta}-\frac{\partial J_\theta}{\partial z}=-\sigma c^{-1}h\omega\sin\lambda\cos\mu\sin\theta \tag{47}$$

The continuity requirement (eq. (2)) reduces to

$$\nabla\cdot\mathbf{J}=\frac{\partial J_\theta}{r\partial\theta}+\frac{\partial J_z}{\partial z}=0 \tag{48}$$

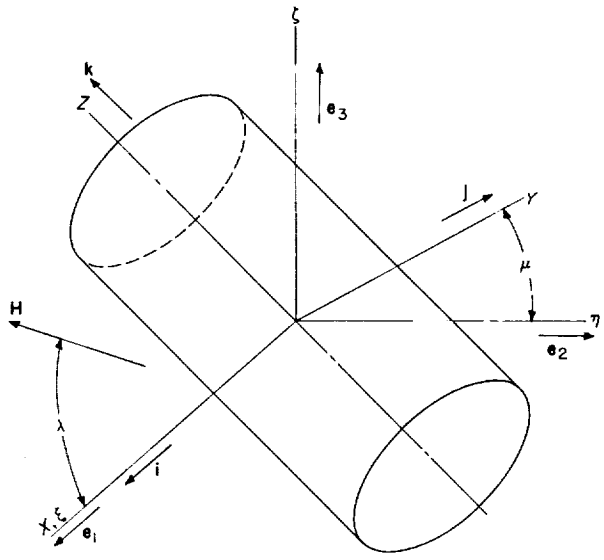

FIGURE 10. Coordinate systems for tumbling cylinder.

Radial current having been neglected, the boundary condition is simply

$$J_z=0 \qquad \left(z=\pm\frac{l}{2}\right) \tag{49}$$

This problem could be solved by a scalar potential as before. However, to demonstrate an alternate approach, the solution will be by means of a stream function. With a stream function ψ defined as before (see eq. (20))

$$\nabla^2\psi=-(\nabla\times\mathbf{J})_r \tag{50}$$

so that, by equation (47),

$$\nabla^2\psi=\frac{\partial^2\psi}{r^2\partial\theta^2}+\frac{\partial^2\psi}{\partial z^2}=\sigma c^{-1}h\omega\sin\lambda\cos\mu\sin\theta \tag{51}$$

Solving equation (51) yields

$$\psi=\sigma c^{-1}h\omega r^3\sin\lambda\cos\mu\sin\theta + \sum_{n=0}^{\infty}(A_n\sin n\theta+B\cos n\theta)\left(C_n\sinh\frac{nz}{r}+D_n\cosh\frac{nz}{r}\right) \tag{52}$$

Only the sin θ component of the harmonic part of ψ will not vanish when the boundary condition is applied; therefore, $A_n=0$ $(n>1)$ and $B_n=0$. By symmetry $C_n=0$. The current density is then calculated by equations (50) and (52), under the condition that the longitudinal component vanish at the ends (eq. (49)), and A_1D_1 is

thereby determined. Thus the stream function and current components are shown to be

$$\psi(\theta, z)=\sigma c^{-1}h\omega l^3 \sin\lambda\cos\mu\left(1-\frac{\cosh\frac{z}{r}}{\cosh\frac{l}{2r}}\right)\sin\theta \quad (53)$$

$$J_\theta=\sigma c^{-1}h\omega r^2\sin\lambda\cos\mu\frac{\sinh\frac{z}{r}}{\cosh\frac{l}{2r}}\sin\theta \quad (54)$$

$$J_z=\sigma c^{-1}h\omega r^2\sin\lambda\cos\mu\left(1-\frac{\cosh\frac{z}{r}}{\cosh\frac{l}{2r}}\right)\cos\theta \quad (55)$$

The torque resulting from this current is

$$\mathbf{L}=\pi\sigma c^{-2}h^2\omega\sin\lambda r^3 l\tau\left(1-\frac{2r}{l}\tanh\frac{l}{2r}\right)\cos\mu(-\mathbf{i}\sin\lambda\cos\mu+\mathbf{k}\cos\lambda) \quad (56)$$

Expressed in space-fixed axes,

$$\mathbf{L}=\pi\sigma c^{-2}h^2\omega\sin\lambda r^3 l\tau\left(1-\frac{2r}{l}\tanh\frac{l}{2r}\right)(-\mathbf{e}_1\sin\lambda\cos^2\mu-\mathbf{e}_2\cos\lambda\sin\mu\cos\mu+\mathbf{e}_3\cos\lambda\cos^2\mu) \quad (57)$$

Averaging this torque around one revolution gives simply

$$\mathbf{L}_{av}=\frac{\pi}{2}\sigma c^{-2}h^2\omega\sin\lambda r^3 l\tau\left(1-\frac{2r}{l}\tanh\frac{l}{2r}\right)(-\mathbf{e}_1\sin\lambda+\mathbf{e}_3\cos\lambda) \quad (58)$$

Comparison of equation (58) for a tumbling cylinder with equation (19) for a symmetrically spinning cylinder shows the two expressions to be identical except for a factor of 1/2 in the case of the tumbling cylinder because of the sinusoidal variation of the current. Also, it is seen from equations (21) and (53) that the streamlines are identical.

THIN-WALLED CONES AND CONIC FRUSTUMS

In studying the magnetic torques on thin-walled symmetrically spinning cones and cone frustums, coordinate systems are set up as shown in figure 11. Cartesian and polar coordinates are oriented

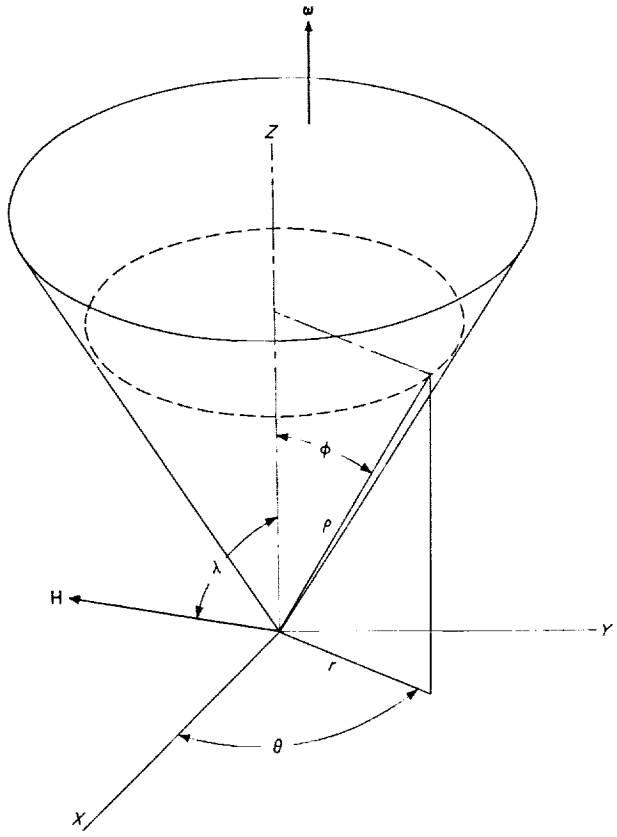

FIGURE 11.—Coordinate systems for cone.

as before, the Z-axis being parallel to $\boldsymbol{\omega}$, the X, Z plane containing $\mathbf{H}$, θ being measured in the X, Y plane from the X-axis, and r being measured normal to the Z-axis. The origin is placed at the vertex of the cone. The cone half-angle is ϕ. In addition, ρ is defined as the distance from the vertex to a point on the cone, and unit vectors $\mathbf{u}_\phi$ and $\mathbf{u}_\rho$ are defined normal to ρ and $\mathbf{u}_\theta$ and parallel to ρ, respectively.

As before, only the component of $\nabla\times\mathbf{J}$ normal to the surface is considered. Equation (1) gives

$$(\nabla\times\mathbf{J})_\phi=-\sigma c^{-1}h\omega\sin\lambda\cos\phi\sin\theta \quad (59)$$

which is the governing equation for a conical surface.

As with the cylinder, the cone or cone frustum is a developable surface and can be rolled out on a plane; therefore, the problem becomes a boundary-value problem in a sector of an annulus or of a circle in a plane. The polar coordinates in the plane are the radial distance ρ and the central angle ν, which is related to the angle θ by the

equation

$$\nu=\theta \sin \phi \tag{60}$$

(This equation is readily verified by noting that a circumferential distance $(\rho \sin \phi)\theta$ on the cone becomes $\rho\nu$ in the plane.)

In polar coordinates, the Laplacian of the stream function is given by

$$\nabla^2\psi=\frac{\partial^2\psi}{\partial\rho^2}+\frac{\partial\psi}{\rho\partial\rho}+\frac{\partial^2\psi}{\rho^2\partial\nu^2}$$

so that equation (59) now becomes, with the aid of equation (60),

$$\frac{\partial^2\psi}{\partial\rho^2}+\frac{\partial\psi}{\rho\partial\rho}+\frac{1}{\rho^2\sin^2\phi}\frac{\partial^2\psi}{\partial\theta^2}=\sigma c^{-1}h\omega \sin\lambda\cos\phi\sin\theta \tag{61}$$

As in the case of symmetrically spinning cylinders, only the $\sin\theta$ term of ψ remains after the boundary conditions have been applied.

Accordingly, the solution of equation (61) is assumed to be of the form

$$\psi(\rho,\theta)=\sin\theta f(\rho) \tag{62}$$

Substituting this expression into equation (61) and rewriting gives

$$\rho^2\frac{d^2f}{d\rho^2}+\rho\frac{df}{d\rho}-\csc^2\phi f=\sigma c^{-1}h\omega\sin\lambda\cos\phi\rho^2 \tag{63}$$

The result is seen to be an equidimensional equation. Substituting the solution for $f(\rho)$ into equation (62) gives

$$\psi(\rho,\theta)=\frac{\sigma c^{-1}h\omega\sin\lambda\cos\phi\sin\theta}{4-\csc^2\phi}(\rho^2+A\rho^{\csc\phi}+B\rho^{-\csc\phi}) \tag{64}$$

where A and B are to be determined.

The two components of current density are

$$\frac{\partial\psi}{\partial\rho}=J_\theta(\rho,\theta)=\frac{\sigma c^{-1}h\omega\sin\lambda\cos\phi\sin\theta}{4-\csc^2\phi}(2\rho+A\csc\phi\rho^{\csc\phi-1}-B\csc\phi\rho^{-\csc\phi-1}) \tag{65}$$

$$-\frac{1}{\rho\sin\phi}\frac{\partial\psi}{\partial\theta}=J_r(\rho,\theta)=-\frac{\sigma c^{-1}h\omega\sin\lambda\cot\phi\cos\phi}{4-\csc^2\phi}(\rho+A\rho^{\csc\phi-1}+B\rho^{-\csc\phi-1}) \tag{66}$$

In applying these equations to a cone, the boundary conditions are that $J_\rho=0$ at the end $\rho=\rho_a$ and that the current density remains finite throughout the cone. By the latter condition $B=0$, and the former gives

$$\rho_a+A\rho_a^{\csc\phi-1}=0$$

or

$$A=-\rho_a^{2-\csc\phi} \tag{67}$$

For a cone frustum, it is required that $J_\rho=0$ at both ends, $\rho=\rho_a$ and $\rho=\rho_b$. Thus

$$\rho_a+A\rho_a^{\csc\phi-1}+B\rho_a^{-\csc\phi-1}=0 \tag{68a}$$

$$\rho_b+A\rho_b^{\csc\phi-1}+B\rho_b^{-\csc\phi-1}=0 \tag{68b}$$

Simultaneous solution of these two equations gives

$$A=\frac{\rho_a^{-\csc\phi-1}\rho_b-\rho_a\rho_b^{-\csc\phi-1}}{\rho_a^{\csc\phi-1}\rho_b^{-\csc\phi-1}-\rho_a^{-\csc\phi-1}\rho_b^{\csc\phi-1}} \tag{69a}$$

$$B=\frac{\rho_a\rho_b^{\csc\phi-1}-\rho_a^{\csc\phi-1}\rho_b}{\rho_a^{\csc\phi-1}\rho_b^{-\csc\phi-1}-\rho_a^{-\csc\phi-1}\rho_b^{\csc\phi-1}} \tag{69b}$$

Substitution of the current expressions (eqs. (65) and (66)) into equation (18) gives the torque:

$$\mathbf{L}=\frac{\pi\sigma c^{-2}h^2\omega\sin\lambda\cos^2\phi\sin\phi\tau}{4-\csc^2\phi}\left(\frac{\rho^4}{4}+\frac{A\rho^{\csc\phi+2}}{\csc\phi+2}+\frac{B\rho^{-\csc\phi+2}}{-\csc\phi+2}\right)\Bigg|_{\rho_a}^{\rho_b}(-\mathbf{i}\cos\lambda+\mathbf{k}\sin\lambda) \tag{70}$$

It is seen that the solution in the form given here contains a singularity for $\csc\phi=\pm2$ or $\phi=\pm30°$. This is due to the homogeneous part of the solution becoming identical with the inhomogeneous part. The solution for this case may be obtained by introducing a transformation variable w defined by

$$\left.\begin{aligned}\rho&=e^w\\ w&=\log_e\rho\end{aligned}\right\} \tag{71}$$

whence

$$\rho\frac{df}{d\rho}=\frac{df}{dw}$$

$$\rho^2\frac{d^2f}{d\rho^2}=\frac{d^2f}{dw^2}-\frac{df}{dw}$$

With these expressions, equation (63) gives, for $\phi=\pm30°$,

$$\frac{d^2f}{dw^2}-4f=\sigma c^{-1}h\omega\sin\lambda\frac{\sqrt{3}}{2}e^{2w}$$

The solution of this equation is

$$f=\frac{\sqrt{3}}{8}\sigma c^{-1}h\omega \sin\lambda(we^{2w}+Ae^{2w}+Be^{-2w})$$
$$=\frac{\sqrt{3}}{8}\sigma c^{-1}h\omega \sin\lambda(\rho^2\log_e\rho+A\rho^2+B\rho^{-2}) \quad (72)$$

The stream function is thus given by

$$\psi(\rho,\theta)=\frac{\sqrt{3}}{8}\sigma c^{-1}h\omega \sin\lambda \sin\theta(\rho^2\log_e\rho+A\rho^2+B\rho^{-2}) \quad (73)$$

and the current density components are

$$J_\theta(\rho,\theta)=\frac{\sqrt{3}}{8}\sigma c^{-1}h\omega \sin\lambda \sin\theta[\rho(1+\log_e\rho)+2A\rho-2B\rho^{-3}] \quad (74)$$

$$J_\rho(\rho,\theta)=-\frac{\sqrt{3}}{4}\sigma c^{-1}h\omega \sin\lambda \cos\theta(\rho\log_e\rho+A\rho+B\rho^{-3}) \quad (75)$$

As before, these equations are applied to a cone, and the constants are found to be

$$A=-\log_e\rho_a$$
$$B=0$$

Likewise, for a frustum, the constants are

$$A=\frac{\rho_b^4\log_e\rho_b-\rho_a^4\log_e\rho_a}{\rho_a^4-\rho_b^4}$$
$$B=\frac{\rho_a^4\rho_b^4(\log_e\rho_a-\log_e\rho_b)}{\rho_a^4-\rho_b^4}$$

The resultant torque is then

$$\mathbf{L}=\frac{3}{16}\pi\sigma c^{-2}h^2\omega \sin\lambda\tau\left[\frac{1}{3}\rho^3\left(\log_e\rho-\frac{1}{3}\right)+\frac{1}{2}A\rho^2-\frac{1}{2}B\rho^{-2}\right](\mathbf{i}\cos\lambda-\mathbf{k}\sin\lambda) \quad (76)$$

SERIES OF CONE FRUSTUMS

If a series of m conic frustums are joined end to end, as in figure 12, equations (64), (65), and (66) apply in each section, and it remains only to determine the A and B for each section in order to define fully the current and hence the torque. At the joint, the radial component of current must be continuous, and the circumferential component must also be continuous as otherwise

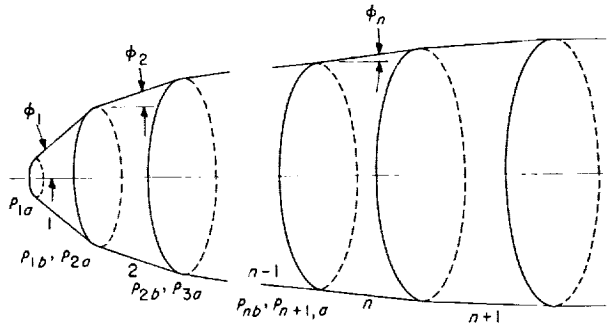

FIGURE 12.—Series of cone frustums.

a vortex line would be formed, with resulting infinite curl of current along the joint. Therefore, the conditions for determining the constants are that the respective components of current are continuous at the joints, and that at an open end the radial component vanishes, or that, if the end is closed by a cone, the current remains finite. With the notation for the ends of each section as shown in figure (12), these conditions can be written for the junctions as

$$J_\rho(\rho_{nb},\theta)=J_\rho(\rho_{n+1,a},\theta) \quad (77a)$$

$$J_\theta(\rho_{nb},\theta)=J_\theta(\rho_{n+1,a},\theta) \quad (77b)$$

By using equations (65) and (66), equations (77) become

$$A_n a_{nb}+B_n b_{nb}+c_{nb}=A_{n+1}a_{n+1,a}+B_{n+1}b_{n+1,a}+c_{n+1,a} \quad (78a)$$

$$A_n a_{nb}-B_n b_{nb}+f_{nb}=A_{n+1}a_{n+1,a}-B_{n+1}b_{n+1,a}+f_{n+1,a} \quad (78b)$$

where

$$a_{na}=\frac{\rho_{na}^{\csc\phi_n-1}\cot\phi_n}{4-\csc^2\phi_n} \quad (79a)$$

$$b_{na}=\frac{\rho_{na}^{-\csc\phi_n-1}\cot\phi_n}{4-\csc^2\phi_n} \quad (79b)$$

$$c_{na}=\frac{\rho_{na}\cot\phi_n}{4-\csc^2\phi_n} \quad (79c)$$

$$f_{na}=\frac{2\rho_{na}\cos\phi_n}{4-\csc^2\phi_n} \quad (79d)$$

and a_{nb}, b_{nb}, c_{nb}, and f_{nb} are similarly defined. The two parts of equation (78) give, by addition and subtraction,

$$A_n a_{nb}+\frac{c_{nb}+f_{nb}}{2}=A_{n+1}a_{n+1,a}+\frac{c_{n+1,a}+f_{n+1,a}}{2} \quad (80a)$$

$$B_n b_{nb}+\frac{c_{nb}-f_{nb}}{2}=B_{n+1}b_{n+1,a}+\frac{c_{n+1,a}-f_{n+1,a}}{2} \quad (80b)$$

In the application of these equations, it is important to note that, in proceeding from one end of the frustum series to the other, if the opening angle of a cone with radius increasing with the distance along the body is considered positive, the opening angle of a cone with radius decreasing as z increases must be negative, and vice versa. This sign convention is intrinsically assumed by the equations.

Equations (80) furnish $2m-2$ of the equations necessary for the determination of the $2m$ constants. In order to set up the remaining two equations, it is necessary to consider the following three cases, each of which must be treated separately:

(1) Both ends closed: In this case, finiteness requires that

$$B_1=0 \quad (81a)$$

$$A_m=0 \quad (81b)$$

Equation (81a) provides an initial value from which successive B_n values can be calculated by the recurrence equation (80b). Likewise the A_n values can be determined by equations (80a) and (81b).

(2) One end open and one end closed: At the closed end, finiteness requires that

$$B_1=0$$

and, at the open end, the requirement that the longitudinal current vanish gives equation (68b) applied to the mth segment. Thus, the B_n values can again be calculated by recurrence, after which equation (68b) gives A_m, and the A_n values can then be determined similarly.

(3) Both ends open: The boundary conditions for this case are that the radial component of the current vanish at each end, so that equations (68a) and (68b) are applied to the first and last segments, respectively. Next A_m and B_m are expressed by linear relations in A_1 and B_1, respectively, obtained by successive use of equations (80a) and (80b). Equations (68a) and (68b) now become a pair of simultaneous equations in A_1 and B_1, so that these two can be found. The others then follow.

The constants in the current equations having been determined, the flow is completely defined and the torque follows by summing the contributions of all the sections, each being determined by equation (70).

GENERAL THIN-WALL BODY OF REVOLUTION

The next step is to apply the theory developed for series of frustums to the case of a continuous body of revolution (fig. 13) having as generatrix an arbitrary curve, say $r=r(z)$, which has a piecewise continuous first derivative dr/dz. Initially, however, it will be assumed that dr/dz is continuous throughout the length of the body.

The body is considered as made up of a large number of frustums joined; therefore, equations (80) apply. Equation (80a) is now rewritten in the following form (for a reason that will be immediately apparent):

$$A_{n+1}a_{n+1,a}-A_n a_{nb} =\frac{1}{2}[(c_{nb}-c_{n+1,a})+(f_{nb}-f_{n+1,a})] \quad (82)$$

If the body is considered to be continuously curved,

$$A_{n+1}=A_n+\frac{dA_n}{dz}\Delta z_n$$

$$a_{n+1,a}=a_{nb}+\frac{da_n}{dz}\Delta z_n$$

With these expressions, equation (82) becomes, in the limit,

$$d[a(z)A(z)]=-\frac{1}{2}[dc(z)+df(z)] \quad (83)$$

The subscripts are no longer needed, as A, a, c, and f are continuous functions of z. Equation (83) may be integrated directly to give

$$a(z)A(z)=-\frac{c(z)+f(z)}{2}+a(0)A(0) +\frac{c(0)+f(0)}{2} \quad (84)$$

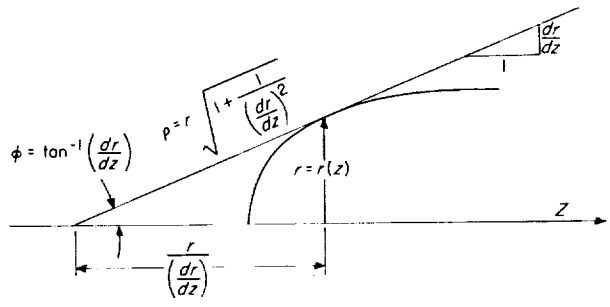

FIGURE 13.—Geometry of general body of revolution.

or

$$A(z)=a^{-1}(z)\left[a(0)A(0)+\frac{c(0)+f(0)}{2}-\frac{c(z)+f(z)}{2}\right] \quad (85)$$

Similarly,

$$B(z)=b^{-1}(z)\left[b(0)B(0)+\frac{c(0)+f(0)}{2}-\frac{c(z)-f(z)}{2}\right] \quad (86)$$

The quantities a, b, c, and f are defined by equations (79) as functions of ρ and ϕ. These are defined in terms of $r(z)$ by the geometry of the problem, as shown in figure (13), as

$$\rho=r\sqrt{1+\left(\frac{dr}{dz}\right)^{-2}} \quad (87)$$

$$\phi=\tan^{-1}\left(\frac{dr}{dz}\right) \quad (88)$$

Other needed relations that follow from figure 13 are

$$\csc^2\phi=1+\left(\frac{dr}{dz}\right)^{-2}$$

$$\cot\phi=\left(\frac{dr}{dz}\right)^{-1}$$

The constants $A(0)$ and $B(0)$ are determined in the same manner as that outlined for the joined frustums, in order to satisfy the condition that no current flows out the ends. The functions $A(z)$ and $B(z)$ thus evaluated are substituted into equations (64), (65), and (66) to obtain the stream function and current components. The torque then follows as

$$\mathbf{L}=\pi\sigma c^{-2}h^2\omega\mathbf{k}\int_{\rho_a}^{\rho_b}\frac{\cos^2\phi\sin\phi}{4-\csc^2\phi}\left[\rho^3+A(z)\rho^{\csc\phi+1}+B(z)\rho^{-\csc\phi+1}\right]d\rho \quad (89)$$

In general, this integral would have to be evaluated numerically. Any discontinuities in the slope are accounted for merely by treating the discontinuity as a juncture in a series of frustums.

NUMERICAL EXAMPLE

As an example of the application of the formulas of this paper, the magnetic torque acting on an aluminum cylinder such as the heat shield of the micrometeoroid satellite S–55 in a symmetrical spin is calculated. For the calculations, the following numbers are used:

$h=0.30$ gauss
$\omega=21.0$ radians/sec
$l=96$ cm
$r=24$ cm
$\tau=0.05$ cm
$c=3\times10^{10}$ cm/sec
$\sigma=0.312\times10^{6}$ (ohm-cm)$^{-1}$
$\lambda=90°$

The fineness ratio is 2, for which $1-\frac{2r}{l}\tanh\frac{l}{2r}=0.52$.

It is necessary to express σ in Gaussian units, that is, in (statohms-cm)$^{-1}$. The torque is then calculated by equation (19) as:

$$\mathbf{L}=-\mathbf{k}\pi\times2.81\times10^{17}\times\frac{(0.3)^2\times21.0}{9\times10^{20}}\times24^3\times96\times0.05\times0.52$$

$$=-64.0\mathbf{k}\text{ dyne-cm}$$

RÉSUMÉ

A theoretical analysis has been made of the eddy currents induced by an applied magnetic field on the following spinning shapes:

(1) Thin-wall symmetrically spinning cylinder,
(2) Thick-wall symmetrically spinning cylinder,
(3) Thin-wall tumbling cylinder,
(4) Thin-wall cone and cone frustum,
(5) Joined thin-wall cone frustums, and
(6) General thin-wall body of revolution.

From the current expressions, the torques are calculated. The first two cases were solved by applying boundary conditions to the scalar potential of the electric field. The other cases were solved by means of a stream function.

Figures that show the variation of torque with fineness ratio and thickness ratio are presented for thin- and thick-wall cylinders. From these, the degree of approximation in the thin-wall treatment can be ascertained. It was found that the average torque acting on a tumbling cylinder is one-half the torque acting on a symmetrically spinning cylinder, all other factors being equal.

LANGLEY RESEARCH CENTER,
NATIONAL AERONAUTICS AND SPACE ADMINISTRATION,
LANGLEY STATION, HAMPTON, VA., *October 12, 1961.*

REFERENCES

1. Rosenstock, Herbert B.: The Effect of the Earth's Magnetic Field on the Spin of the Satellite. Astronautica Acta, Vol. III, Fasc. 3, 1957, pp. 215–221.
2. Zonov, Yu. V.: On the Problem of the Interaction Between a Satellite and the Earth's Magnetic Field. NASA TT F–37, 1960.
3. Bandeen, W. R., and Manger, W. P.: Angular Motion of the Spin Axis of the Tiros I Meteorological Satellite Due to Magnetic and Gravitational Torques. NASA TN D–571, 1961.
4. Vinti, John P.: Theory of the Spin of a Conducting Satellite in the Magnetic Field of the Earth. Rep. No. 1020, Ballistic Res. Labs., Aberdeen Proving Ground, July 1957.
5. Smythe, William R.: Static and Dynamic Electricity. McGraw-Hill Book Co., Inc., 1939.
6. Morse, Philip M., and Feshbach, Herman: Methods of Theoretical Physics. McGraw-Hill Book Co., Inc., 1953.
7. Jahnke, Eugene, and Emde, Fritz: Tables of Functions With Formulae and Curves. Rev. ed., Dover Publications, 1943.

U.S. GOVERNMENT PRINTING OFFICE:1962